Journal of Computational Physics 229 (2010) 7361–7372

Contents lists available at ScienceDirect

Journal of Computational Physics

journal homepage: www.elsevier.com/locate/jcp

A nonconforming finite element method for the Cahn–Hilliard equation

Shuo Zhang [a], Ming Wang [b,*]

[a] LSEC, Institute of Computational Mathematics, Academy of Mathematics and Systems Science, Chinese Academy of Sciences, Beijing 100080, PR China
[b] LMAM School of Mathematical Sciences, Peking University, Beijing 100871, PR China

ARTICLE INFO

Article history:
Received 21 September 2009
Received in revised form 29 May 2010
Accepted 12 June 2010
Available online 18 June 2010

Keywords:
Cahn–Hilliard equation
Nonconforming finite element
Convexity splitting
Phase transition

ABSTRACT

This paper reports a fully discretized scheme for the Cahn–Hilliard equation. The method uses a convexity-splitting scheme to discretize in the temporal variable and a nonconforming finite element method to discretize in the spatial variable. And, the scheme can preserve the mass conservation and energy dissipation properties of the original problem. Some typical phase transition phenomena are also observed through the numerical examples.

1. Introduction

This paper is devoted to the numerical method for the Cahn–Hilliard equation, which is a fourth-order nonlinear parabolic diffusion equation of the type

$$\frac{\partial u}{\partial t} = -\varepsilon^2 \Delta^2 u + \Delta \varphi(u), \tag{1}$$

where u is a function in the spatial variable x and temporal variable t.

The Cahn–Hilliard equation was first introduced by Cahn and Hilliard in the 1950s, in order to model the spinodal decomposition[1] phenomenologically [4,5]. The equation has since become important, especially in applied sciences where it is used frequently [1,3,28,36]. In literatures u can stand for an order parameter or other phase variable of physical meaning.

Attempts to solve the Cahn–Hilliard equation numerically have a long history, which can be dated back to Langer, Bar-on and Miller's 1975 study [31]. In this research, the Cahn–Hilliard equation was solved numerically for numerical modeling and simulation of phase transition phenomena. Elliott and French's paper [14] is one of the earliest works totally devoted to numerically solving the Cahn–Hilliard equation, though Elliott and Zheng had mentioned the Galerkin approximation of the Cahn–Hilliard equation in a slightly earlier study [18].

Numerous studies have been published on the numerical solution of the Cahn–Hilliard equation during the past 20 years. Elliott and French [14] discussed the spline finite element method for the 1D problem, and offered a fully discretized method with their theoretical analysis. When higher-dimensional spaces are taken into account, however, it is much more difficult to construct finite element space with full continuity. In [15], Elliott and French made use of the famous Morley element for

* Corresponding author. Tel.: +86 10 62651389.
E-mail addresses: szhang@lsec.cc.ac.cn (S. Zhang), mwang@math.pku.edu.cn (M. Wang).

[1] Spinodal decomposition is a phenomenon frequently encountered in the material sciences. For instance, as reported in [35], as the homogeneous Al-rich Al–Zn alloy is rapidly quenched from 400 to 100 °C, the alloy would separate into a distinct Al-rich part and a distinct Zn-rich part. This is a typical spinodal decomposition phenomenon.

0021-9991/$ - see front matter © 2010 Elsevier Inc. All rights reserved.
doi:10.1016/j.jcp.2010.06.020

constructing finite element space, and presented a semi-discretized scheme; it should be noted, though, that the theoretical analysis therein did not emphasize the impact of characteristic parameters in numerical implementation. The authors of [16] followed the derivation of the conservation law, to rewrite the Cahn–Hilliard equation as a system of second-order problems to be solved numerically by lower-degree polynomials, and they presented both a semi and fully discretized scheme. Second-order splitting methods were also discussed in [10] and [17] in different contexts.

Nevertheless, as pointed out by Du and Nicolaides [11], the validity of the theoretical analysis in [15,16] depends on an assumption, say the boundness of the maximum of the solution, which might not be obviously true for a fully discretized scheme. In the same paper, Du and Nicolaides constructed a numerical method for 1D problem whereby the boundness of the maximum was guaranteed, and they also presented the error analysis.

Besides this early research on the theory of finite element methods for the Cahn–Hilliard equation, some works concentrated on preserving some key properties of the Cahn–Hilliard equation through numerical simulation. Because of the nature of the finite element methods, mass conservation is easily achieved. Energy dissipation is also considered in some works, among which the early ones include [16,11] also [25]. In fact, energy dissipation has become one of the most important criteria for numerical methods. In addition, long-time behavior is also a key feature of the Cahn–Hilliard equation. The long-time behavior of the numerical solution was considered in [13,24].

So far, finite element methods for the Cahn–Hilliard equation have elicited the research focused on the numerical method for other problems. For example, Blowey and Barrett developed finite element methods for some nonstandard Cahn–Hilliard-type equations; see, e.g., [2] and the references therein. Feng and coauthors developed the conforming and mixed finite element method for the Cahn–Hilliard equation, and considered further some other models as the asymptotic limit of the equations; adaptive techniques were also introduced; see [21–23] and references therein. The discretization of a Navier-stokes and Cahn-Hilliard system was discussed in [30]. We also noted that a surface finite element method was presented in [12] to numerically solve the surface Cahn–Hilliard equation defined on hypersurfaces.

Some other methods were involved into the numerical solution of Cahn–Hilliard equation as well. Over time, the finite difference method has been used for most practical computation.[2] However, few works have focused on the theoretical analysis of using this method. We refer to [37,7,8,26,27] for the development of use of the method. The spectral and quasi-spectral methods are also used frequently. We refer to [43–45] for some nonlinear energy dissipative methods based on spectral methods by Ye and others. We also refer to [6,47] by Chen and Shen, and [29] by He, Liu and Tang for some linear schemes. The discontinuous Galerkin method is relatively new; however, it has been used in [9,39,20,40] for the Cahn–Hilliard equation and extended to more general applications to systems coupled with the Allen–Cahn and Cahn–Hilliard equations [41].

In this paper, we consider the nonconforming finite element method for the fourth-order problem directly. Because the interfacial energy parameter ε (see Eq. (1)) can be small in practice, in general, the performance of a nonconforming method that does not work for second-order problems will be limited. To date, few studies have reported the numerical implementation of the nonconforming method.

Currently, we consider the initial-boundary value problem of the Cahn–Hilliard equation in the 2D domain, and present a numerical method based on the nonconforming finite element method. For the spatial variable, we use a nonconforming finite element method and discretize the fourth-order problem directly; for the temporal variable, we use of linear semi-implicit convexity-splitting scheme. The remainder of the paper is organized as follows. The next section offers some preliminary observations about the Cahn–Hilliard equation. The fully discretized scheme is presented in Section 3, and some numerical examples are given in Section 4. Finally, Section 5 offers concluding remarks and additional comments.

2. The Cahn–Hilliard equation

In this paper, we consider the Cahn–Hilliard equation of the type

$$\frac{\partial u}{\partial t} = -\varepsilon^2 \Delta^2 u + \Delta W'(u), \tag{2}$$

where ε is a parameter that is small in general; Δ is the Laplacian operator; $W(\cdot)$ is a nonconvex function with double well structure; qualitatively

$$W(u) = \frac{\gamma}{4}(u^2 - 1)^2,$$

where γ is a parameter to illustrate the altitude of the bulk energy.

The solution of (2) is a distribution function with respect to the spatial and temporal variables; it is called the phase variable in sequel. The functional of variable u

$$E(u) = \int_\Omega \left(\frac{\varepsilon^2}{2} |\nabla u|^2 + W(u) \right) \tag{3}$$

[2] "Due to its simplicity and small memory requirement, most of the existing phase-field simulations employed the explicit forward Euler method in time and finite-difference in space" [6].

is called the Cahn–Hilliard free energy. Note that the Cahn–Hilliard free energy is the sum of two distinct parts: bulk energy, which is independent of the spatial gradient of the phase variable, and interfacial energy, which depends on the gradient in the spatial variable. The Cahn–Hilliard equation describes the dissipation of Cahn–Hilliard free energy in a conservative system. In fact, the equation fulfills the two fundamental properties,

– local mass conservation of the phase variable,

$$\frac{\partial u}{\partial t} = -\nabla \cdot \vec{j}, \quad \vec{j} = \varepsilon^2 \nabla \Delta u + \nabla W'(u); \tag{4}$$

– dissipation of the Cahn–Hilliard free energy,

$$\vec{j} = \frac{\delta E}{\delta u}. \tag{5}$$

The Cahn–Hilliard equation describes the evolution of the phase variable, which obeys the free energy minimization law, and it describes the different roles played by the two parts at different stages. The equation presents the whole process as one of competition between the two parts.

When Cahn and Hilliard first introduced the equation to model the spinodal decomposition, they viewed the phenomenon as being the decrease of nonconvex energy functional under the restriction of the mass conservation law; they, therefore, set the Cahn–Hilliard equation to govern the process. So far, because of its ability to illustrate the mass and energy properties, and the characteristics of the interface-moving structure of the solution, the Cahn–Hilliard equation has been used widely in the applied sciences, where it has become a fundamental equation.

Let $\Omega \subset \mathbb{R}^2$ be a bounded domain, $\partial\Omega$ the boundary of Ω, and n the unit outer normal vector of $\partial\Omega$. In this paper, we consider the initial-boundary value problem of the Cahn–Hilliard equation as the model problem:

$$\begin{cases} \frac{\partial u}{\partial t} = -\varepsilon^2 \Delta^2 u + \Delta W'(u), & x \in \Omega, \\ \partial_{\mathrm{n}} u = \partial_{\mathrm{n}} \Delta u = 0, & x \in \partial\Omega, \\ u|_{t=0} = u_0, & x \in \Omega. \end{cases} \tag{6}$$

It is easy to verify the global mass conservation and energy dissipation of the model problem. First, by the Cahn–Hilliard equation,

$$0 = \frac{\mathrm{d}}{\mathrm{d}t}\int_\Omega u \,\mathrm{d}x = \int_\Omega \frac{\partial u}{\partial t}\mathrm{d}x = \int_\Omega \left[-\Delta\left(\varepsilon^2 \Delta u - W'(u)\right)\right]\mathrm{d}x = \int_{\partial\Omega} \left[\partial_{\mathrm{n}}\left(\varepsilon^2 \Delta u - W'(u)\right)\right]\mathrm{d}S. \tag{7}$$

If the function f is smooth, $\partial_{\mathrm{n}} f(u) = f'(u)\partial_{\mathrm{n}} u$; thus (7) is guaranteed by the boundary conditions.

Formally, if the solution $u = u(t,x)$ is smooth, then by divergence theorem, we have that

$$\begin{aligned} \frac{\mathrm{d}}{\mathrm{d}t}E(u(t)) &= \frac{\mathrm{d}}{\mathrm{d}t}\int_\Omega \left[\frac{\varepsilon^2}{2}|\nabla u|^2 + W(u)\right]\mathrm{d}x = \int_\Omega \left(-\varepsilon^2 \Delta u + \varphi(u)\right)\frac{\partial u}{\partial t}\mathrm{d}x = \int_\Omega \left(-\varepsilon^2 \Delta u + \varphi(u)\right)\Delta\left(-\varepsilon^2 \Delta u + \varphi(u)\right)\mathrm{d}x \\ &= -\int_\Omega \left|\nabla\left(-\varepsilon^2 \Delta u + \varphi(u)\right)\right|^2 \mathrm{d}x \leqslant 0; \end{aligned}$$

therefore, for $t_1 > t_2$, $E(u(t_1)) \leqslant E(u(t_2))$. Moreover, if $E(u(t_1)) = E(u(t_2))$, then $u(t) = u^*$ for $t_2 \leqslant t \leqslant t_1$, where u^* is such that $-\varepsilon^2 \Delta u^* + \varphi(u^*) = 0$.

3. A fully discretizatized scheme

For the sake of simple numerical computation, we focus on the linear schemes. Because of the fundamental role that energy dissipation plays in the Cahn–Hilliard equation, we will seek to preserve the energy property for the numerical solution.

3.1. A fully discretized scheme

The simplest linear scheme for the temporal variable is the explicit Euler scheme, and it is indeed the scheme utilized most frequently in practice. However, as the explicit Euler scheme uses the result on the current time step, the mechanism for energy dissipation for the equation is hard to represent. The multistep method [37] was used for compensation, but little effect was observed on preserving energy dissipation. A semi-implicit scheme was utilized in [6], where the implicit scheme was used for the higher-order spatial derivatives, and the explicit scheme was used for lower-order derivatives. The semi-implicit scheme is influential; however, the effect on energy dissipation was not discussed in [6]. Eyre [19] presented a semi-implicit scheme based on the convexity splitting of the energy functional, which performed well in the 1D case, and formed the basis of some subsequent studies. Similar to [19], we make use of a semi-implicit one-step scheme, where the lower-order spatial derivative is treated explicitly, and the higher-order spatial derivative is treated implicitly, with an extra stabilization term added.

Let u^n and u^{n+1} be the approximations, and let the step size be k. The discretization scheme in time reads

$$\frac{u^{n+1}-u^n}{k} = -\varepsilon^2\Delta^2 u^{n+1} + \kappa\Delta u^{n+1} - \kappa\Delta u^n + \Delta W'(u^n), \tag{8}$$

where κ is a parameter to be adjusted for the dissipation of the energy.

Once the equation has been discretized in the temporal variable, we have to solve numerically a fourth-order elliptic perturbation problem at every step. Since we consider the variable ε to be small, we utilize a finite element that works for both the fourth- and second-order problems. Thus for the discretization in the spatial variable, we use the modified Zienkiewicz elements.

Let T be a triangle, and the barycentric coordinates are $\lambda_1, \lambda_2, \lambda_3$. For integers $1 \leqslant i < j \leqslant 3$, and $1 \leqslant k \leqslant 3$, $k \neq i$, $k \neq j$, define

$$q_{ij} = \lambda_i^2\lambda_j - \lambda_i\lambda_j^2 + \left(2(\lambda_i - \lambda_j) + \frac{3(\nabla\lambda_i - \nabla\lambda_j)\cdot\nabla\lambda_k}{\nabla\lambda_k\cdot\nabla\lambda_k}(2\lambda_k - 1)\right)\lambda_1\lambda_2\lambda_3.$$

Denote

$$P_T = P_2(T) + \operatorname{span}\{q_{ij} : 1 \leqslant i < j \leqslant 3\}.$$

Then the modified Zienkiewicz element is defined by (1) the shape of the element is triangle T; (2) the shape of the function space is P_T; and (3) the nodal parameters are the evaluation of the functions and first-order derivatives at the vertices of T. We refer to [38] for a more detailed introduction to the general new Zienkiewicz-type element.

Remark 1. The modified Zienkiewicz element has the same nodal parameters as the original Zienkiewicz element, which does not converge for fourth-order problem on general grids. However, the modified Zienkiewicz element has different shape functions, and it converges for fourth-order problems on general shape regular grids. We refer to [38] for the convergence of this modified Zienkiewicz element for Poisson and biharmonic equations, and refer to [46] for the convergence for fourth-order elliptic perturbation problems.

Let $\mathcal{T}_h$ be a triangulation of Ω, and W^h be the finite element space with respect to the modified Zienkiewicz element

$$W^h = \{w_h \in L^2(\Omega) :\ w_h|_T \in P_T,\ w_h \text{ and both its first-order derivatives are continuous at all vertices of the triangulation}\}.$$

Define

$$V^h = \{w_h \in W^h :\ \partial_n w_h \text{ vanishes at the vertices along boundary}\}.$$

Define for piecewise smooth functions v, w,

$$a_h(v,w) = \sum_{T\in\mathcal{T}_h}\sum_{1\leqslant i,j\leqslant 2}\int_T \frac{\partial^2 v}{\partial x_i\partial x_j}\frac{\partial^2 w}{\partial x_i\partial x_j}, \tag{9}$$

$$b_h(v,w) = \sum_{T\in\mathcal{T}_h}\int_T \nabla v\cdot\nabla w. \tag{10}$$

Let $u_h^0 \in V^h$ be an approximation to u_0, and let δt_n ($n \geqslant 0$) be the stepsize in the temporal variable. Then the fully discretized scheme for problem (6) is to seek $\{u_h^n\}_{n\geqslant 0} \subset V^h$ such that for $n \geqslant 0$,

$$(u_h^{n+1}, v_h) + \varepsilon^2\delta t_n a_h(u_h^{n+1}, v_h) + \delta t_n\kappa b_h(u_h^{n+1}, v_h) = (u_h^n, v_h) + \delta t_n(\gamma+\kappa)b_h(u_h^n, v_h) - \gamma\delta t_n b_h((u_h^n)^3, v_h), \quad \forall v_h \in V^h, \tag{11}$$

where $\kappa > 0$ is a parameter.

Remark 2. As far as we know, W^h possesses a minimal number of total degrees of freedom among the finite element spaces for fourth-order problems; see [38] for details.

3.2. Energy stability and derivation of the scheme

Denote

$$V = \{w \in H^2(\Omega) :\ \partial_\nu w|_{\partial\Omega} = 0\},$$

then the solution of the model problem (6) satisfies

$$\left(\frac{\partial u}{\partial t}, v\right) = \left(\frac{\delta E}{\delta u}, \Delta v\right), \quad \forall v \in V. \tag{12}$$

We consider the one-step scheme; i.e., given that $u_k = u(x,t_k)$, we are to solve approximately $\tilde{u}$ for $u(x,t_k+Dt)$, with $Du := \tilde{u} - u$. Specifically, we consider decomposing E into $E = E_1 + E_2$, and solving $\tilde{u} \in V$ for the equation

$$\left(\frac{\tilde{u}-u_k}{Dt},v\right)=\left(\left.\frac{\delta E_1}{\delta u}\right|_{\tilde{u}},\Delta v\right)+\left(\left.\frac{\delta E_2}{\delta u}\right|_{u_k},\Delta v\right),\quad \forall v\in V. \tag{13}$$

Taking $v\equiv 1$ leads to

$$\int_\Omega \tilde{u}=\int_\Omega u_k,\quad \int_\Omega Du=0. \tag{14}$$

Then

$$\int_\Omega(\Delta_N^{-1}Du)=0,\quad \partial_v\Delta_N^{-1}Du|_{\partial\Omega}=0,$$

where Δ_N^{-1} is the inverse operator of the homogeneous Neumann–Laplace operator. Then

$$\begin{aligned}\left.\frac{\delta E}{\delta u}\right|_{\tilde{u}}(Du)&=\left(\left.\frac{\delta E_1}{\delta u}\right|_{\tilde{u}}+\left.\frac{\delta E_2}{\delta u}\right|_{u_k},Du\right)+\left(\left.\frac{\delta E_2}{\delta u}\right|_{\tilde{u}}-\left.\frac{\delta E_2}{\delta u}\right|_{u_k},Du\right)\\&=\left(\frac{Du}{Dt},\Delta_N^{-1}Du\right)+\left(\left.\frac{\delta E_2}{\delta u}\right|_{\tilde{u}}-\left.\frac{\delta E_2}{\delta u}\right|_{Du},Du\right)\\&=-\frac{1}{Dt}\left(\nabla\Delta_N^{-1}Du,\nabla\Delta_N^{-1}Du\right)+\int_0^1\left.\frac{\delta^2E_2}{\delta u^2}\right|_{u_k+sDu}(Du,Du)\mathrm{d}s.\end{aligned}$$

We then obtain

$$\begin{aligned}E(\tilde{u})-E(u)&=\left.\frac{\delta E}{\delta u}\right|_{\tilde{u}}(Du)-\int_0^1\int_0^s\left.\frac{\delta^2E}{\delta u^2}\right|_{(1-\tau)\tilde{u}+\tau u_k}(Du,Du)\mathrm{d}\tau\,\mathrm{d}s\\&=-\frac{1}{Dt}\left(\nabla\Delta_N^{-1}Du,\nabla\Delta_N^{-1}Du\right)+\int_0^1\left.\frac{\delta^2E_2}{\delta u^2}\right|_{u+sDu}(Du,Du)\mathrm{d}s\\&\quad-\int_0^1\int_0^s\left.\frac{\delta^2E}{\delta u^2}\right|_{(1-\tau)\tilde{u}+\tau u_k}(Du,Du)\mathrm{d}\tau\,\mathrm{d}s.\end{aligned}$$

Thus, a sufficient condition for the splitting scheme to preserve energy dissipation is given below.

Proposition 1. *If there are λ_b and λ^a, with $\lambda^a\leqslant\frac{1}{2}\lambda_b$, such that*

$$\left.\frac{\delta^2E_2}{\delta u^2}\right|_w(Du,Du)\leqslant\lambda^a\|Du\|_0^2 \tag{15}$$

and

$$\left.\frac{\delta^2E}{\delta u^2}\right|_w(Du,Du)\geqslant\lambda_b\|Du\|_0^2, \tag{16}$$

hold for all $w\in\{u_k+s(\tilde{u}-u_k)\colon 0\leqslant s\leqslant 1\}$, then

$$E(\tilde{u})-E(u_k)\leqslant 0.$$

By direct computation,

$$\left.\frac{\delta^2E}{\delta u^2}\right|_v(q,q)=\varepsilon^2\int_\Omega\nabla q\cdot\nabla q+\int_\Omega(3v^2-1)q^2.$$

It, therefore, holds for any v and any $q\neq 0$ that

$$\left.\frac{\delta^2E}{\delta u^2}\right|_v(q,q)\geqslant-\|q\|_0^2.$$

Let us take insight (15). We set $\kappa>0$, and then consider the following decomposition of the energy functional:

$$\begin{cases}E_1(u)=\int_\Omega\left(\frac{\varepsilon^2}{2}\nabla u\cdot\nabla u+\frac{\kappa}{2}u^2\right),\\E_2(u)=\int_\Omega\left(\frac{1}{4}u^4-\frac{1}{2}u^2-\frac{\kappa}{2}u^2\right).\end{cases} \tag{17}$$

It is straightforward that for any $w\in L^\infty(\Omega)$, we can always choose $\kappa>0$, such that E_2 is concave near w, and $\left(\frac{\delta^2E_2}{\delta u^2}|_w(p,p)\right)/(p,p)$ is bounded negative from above, e.g., less than $-1/2$. When κ is chosen so that the condition (15) is sat-

isfied, energy dissipation is guaranteed. Such an energy-splitting strategy and other similar energy-stabilization methods can be found in the literature, e.g., [33,34,3] and also [42,29]. We design the numerical scheme based on (17):

$$\frac{\tilde{u}-u_k}{Dt} = \Delta\frac{\delta E_1}{\delta u}\Big|_{\tilde{u}} + \Delta\frac{\delta E_2}{\delta u}\Big|_{u_k} = \varepsilon^2\Delta^2\tilde{u} + \kappa\Delta\tilde{u} - \kappa\Delta u_k + \gamma\Delta(u_k^3 - u_k). \tag{18}$$

Remark 3. The stability of the numerical scheme (18) depends on a proper choice of κ, while the critical value of κ depends on u_k, Dt and ε in a nonlinear way. However, the value of κ can be verified and adjusted in an a posterior way.

Remark 4. Note that the condition (15) is indeed an assumption of the concavity of E_2. The decomposition of the energy below, which set E_2 as the concave part of the energy, induces a scheme whereby the condition (15) is satisfied unconditionally, namely

$$\begin{cases} E_1(u) = \int_\Omega \left(\frac{\varepsilon^2}{2}\nabla u\cdot\nabla u + \frac{\gamma u^4}{4}\right), \\ E_2(u) = -\int_\Omega \frac{\gamma u^2}{2}. \end{cases} \tag{19}$$

The corresponding numerical scheme is then

$$\frac{\tilde{u}-u}{\delta t} = \varepsilon^2\Delta^2\tilde{u} + \gamma\Delta(\tilde{u}^3) - \gamma\Delta u.$$

To make use of the scheme, we have to solve a nonlinear elliptic equation at each step, which makes the scheme more expensive than (18).

Remark 5. The scheme (18) can be viewed as a first-order semi-implicit with a stability term added on. There have been second-order schemes derived similarly. We refer to [29,37] for details.

4. Numerical examples

In this section, we introduce a series of numerical examples to illustrate the characteristics of the scheme. In Section 4.1, we illustrate the stabilization effect of κ; in Section 4.2, we simulate the typical phase transitions by numerical examples.

4.1. Stabilization effect of κ

We test the stabilization effect of the parameter κ with respect to ε and time step Dt. The model problem is the initial-boundary value problem (6), where $\gamma = 1$ in the formulation of W. The computational domain is the unit square $[0,1]\times[0,1]$, and the grid is a nonuniform shape regular mesh with 22,785 nodes and 45,056 triangles. The initial value is the "+" shape function, which is precisely

$$u_0(x,y) = h(|x-0.5|)h(|y-0.5|) - 0.2,$$

where

$$h(z) = \begin{cases} 1, & 0 \leqslant z \leqslant 0.05, \\ 0.5(1+\sin(10\pi z)), & 0.05 \leqslant z \leqslant 0.15, \\ 0, & 0.15 \leqslant z \leqslant 0.5. \end{cases}$$

As shown in Tables 1–3, for different ε, we let κ and Dt vary, and observe whether the numerical scheme will be energy stable. In the tables, "○" stands for that the scheme is stable, whereas the computation can be carried on for long time, (the evolution has entered coarsening stage) and the energy decreases; "×" stands for that the energy dissipation is violated within a few steps, and the energy blows up.

At first, let $\varepsilon^2 = 0.01$, and let Dt and κ vary. Table 1 presents the observations.

Then, let $\varepsilon^2 = 10^{-5}$, and let Dt and κ vary. Table 2 presents the observations.

Table 1
The stability of the scheme with respect to κ and Dt when $\varepsilon^2 = 0.01$.

Dt	5×10^{-3}	10^{-2}	5×10^{-2}	10^{-1}
$\kappa = 0$	○	○	○	○
$\kappa = 0.5$	○	○	○	○
$\kappa = 1$	○	○	○	○

Table 2
The stability of the scheme with respect to κ and Dt when $\varepsilon^2 = 10^{-5}$.

Dt	10^{-5}	5×10^{-5}	10^{-4}	5×10^{-4}	10^{-3}	10^{-2}
$\kappa = 0$	○	×	×	×	×	×
$\kappa = 0.5$	○	○	○	×	×	×
$\kappa = 1$	○	○	○	○	○	○

Table 3
The stability of the scheme with respect to κ and Dt when $\varepsilon^2 = 10^{-6}$.

Dt	2×10^{-5}	5×10^{-5}	10^{-4}	5×10^{-4}	10^{-3}	10^{-2}
$\kappa = 0$	×	×	×	×	×	×
$\kappa = 0.5$	×	×	×	×	×	×
$\kappa = 1$	○	○	○	○	○	○

Finally, let $\varepsilon^2 = 10^{-6}$, and let Dt and κ vary. Table 3 presents the observations.

It can be observed via the numerical examples that, for the benchmark problem,

1. When ε is big, the energy stability is easy to be preserved even when the time step Dt is quite big; when ε is small, the energy stability is hard to preserve, and the stability effect of κ is relied upon;
2. For cases in which the stability effect of κ is needed, to some extent, the bigger κ is, the bigger the critical value of time step is;
3. The choice of a proper κ for sake of the stability of the scheme depends on the time step and ε.

4.2. Phase transition of the Cahn–Hilliard equation

In this subsection, we illustrate the typical phase separation phenomena of the Cahn–Hilliard equation through numerical examples. To be exact, we simulate the spinodal decomposition phenomenon and the subsequent evolution of the phase variable. Through the examples, we observe the dissipation of the total Cahn–Hilliard energy and the competition between the bulk energy and the interfacial energy.

In the examples, the initial values are all small perturbations added to the uniform phase $u \equiv 0$:

$$u_0 = \varsigma.$$

Since $W''(0) < 0$, the uniform phase lies in the spinodal interval of W, and the distribution function of the small altitude will activate a phase separation if ε is small enough. We will also adjust the coefficients ε and γ (see the definition of W) to change the ratio between the interfacial energy and the bulk energy.

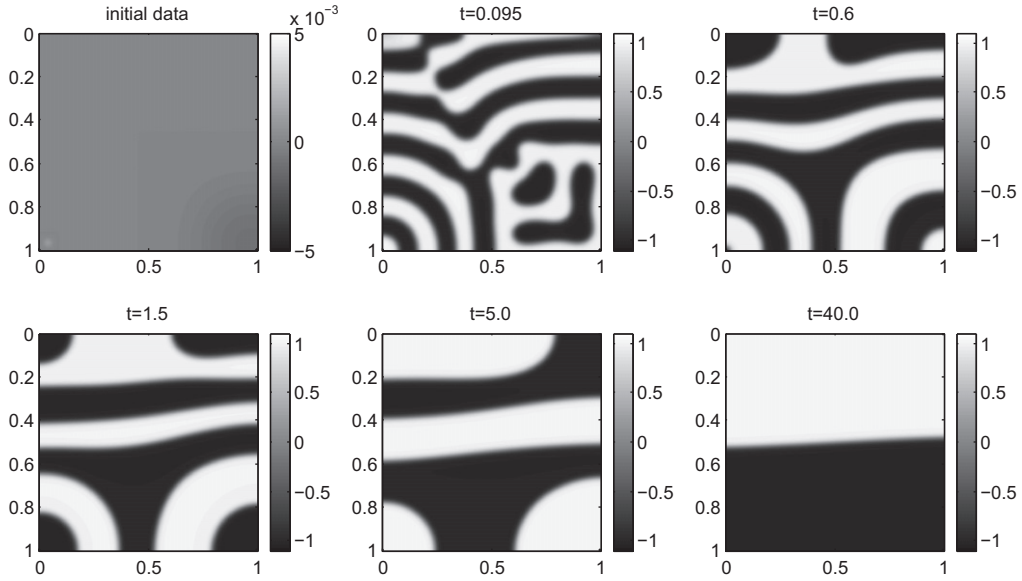

Fig. 1. The phase evolution of Example I. For the initial value, the perturbation is located at two corners.

In the examples, the computation domains are all the unit square $(0,1)\times(0,1)$, with uniform triangulation thereon. There are $100\times100\times2$ triangular cells in all, the scale of the triangulation is $h = 0.01$, and the stepsize is $Dt = 0.001$.

Example I. In this example, $\varepsilon^2 = 10^{-4}$, $\gamma = 1$, and $\kappa = 2$. For the initial value, the perturbation is

$$\varsigma = \begin{cases} 10^{-3}\sin^3(\frac{\pi}{8h}x)\sin^3(\frac{\pi}{8h}y), & (x,y)\in(0,8h)\times(0,8h),\\ -10^{-3}\sin^3(\frac{\pi}{2}x)\sin^3(\frac{\pi}{2}(1-y)), & (x,y)\in(0,1/2)\times(1/2,1). \end{cases}$$

As illustrated by Fig. 1, spinodal decomposition took place at the small perturbation, and was followed by coarsening. After evolving for a long time, the system varied very slowly. Fig. 2 illustrates the evolution of the Cahn–Hilliard energy and the bulk and interfacial energy respectively. The time $t = 0.095$ is when the interfacial energy arrived its maximum.

For the following examples, we define the function G, which is supported on $0\leqslant x-x_0\leqslant T$,

$$G(x,y;x_0,y_0,T) = g_0(x,x_0,T)g_0(y,y_0,T),$$

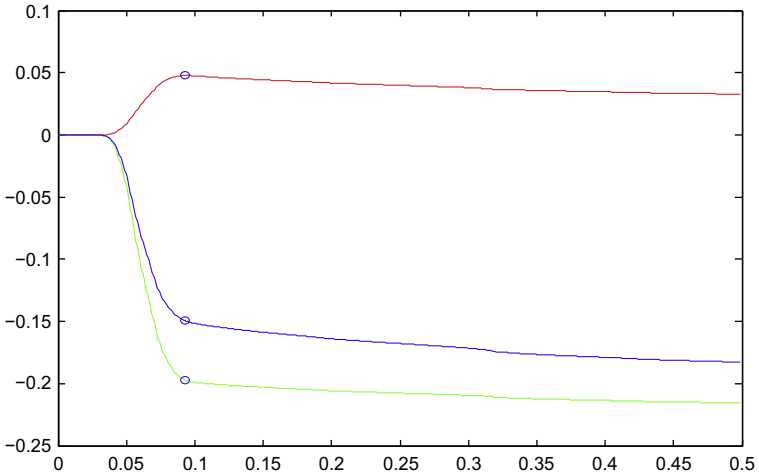

Fig. 2. The energy evolution of Example I. In the figure, the top line is interfacial energy, the middle line is total Cahn–Hilliard energy, and the bottom line is bulk energy.

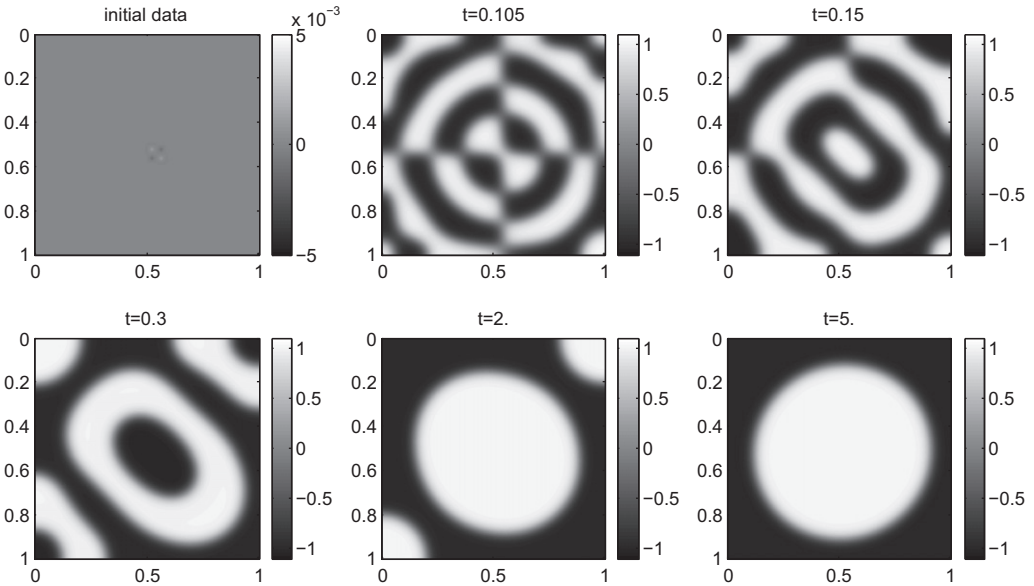

Fig. 3. The phase evolution of Example II. For the initial value, the perturbation is in the middle of the domain.

where the function g_0 is defined by

$$g_0(x, x_0, T) = \sin^3\left(\frac{2\pi}{T}(x - x_0)\right).$$

Example II. In this example, $\varepsilon^2 = 4 \times 10^{-4}$, $\gamma = 1$, and $\kappa = 2$. For the initial value,

$$\varsigma = 10^{-3} G(x, y, 0.5, 0.5, 8h).$$

In this example, we can also observe the typical phase transition phenomena: phase separation–coarsening. In contrast to Example I, because of the bigger interfacial energy density (bigger ε) and the different position of the perturbation, different phase evolution process is observed. See Fig. 3 for the evolution of phase variable and Fig. 4 for the evolution of the energies.

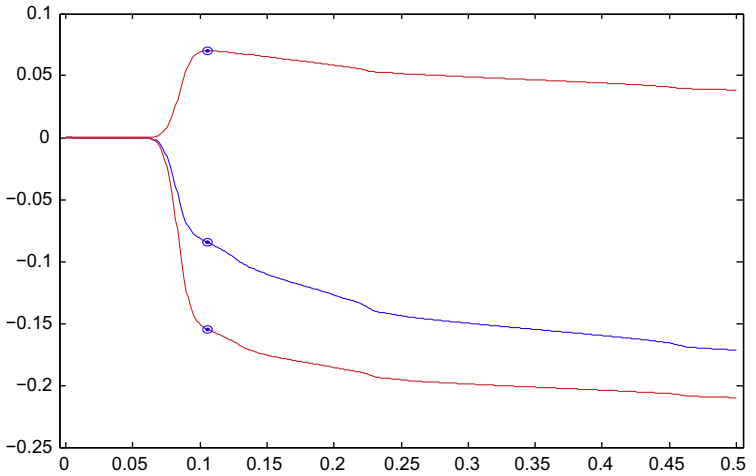

Fig. 4. The energy evolution of Example II. In the figure, the top line is interfacial energy, the middle line is total Cahn–Hilliard energy, and the bottom line is interfacial energy.

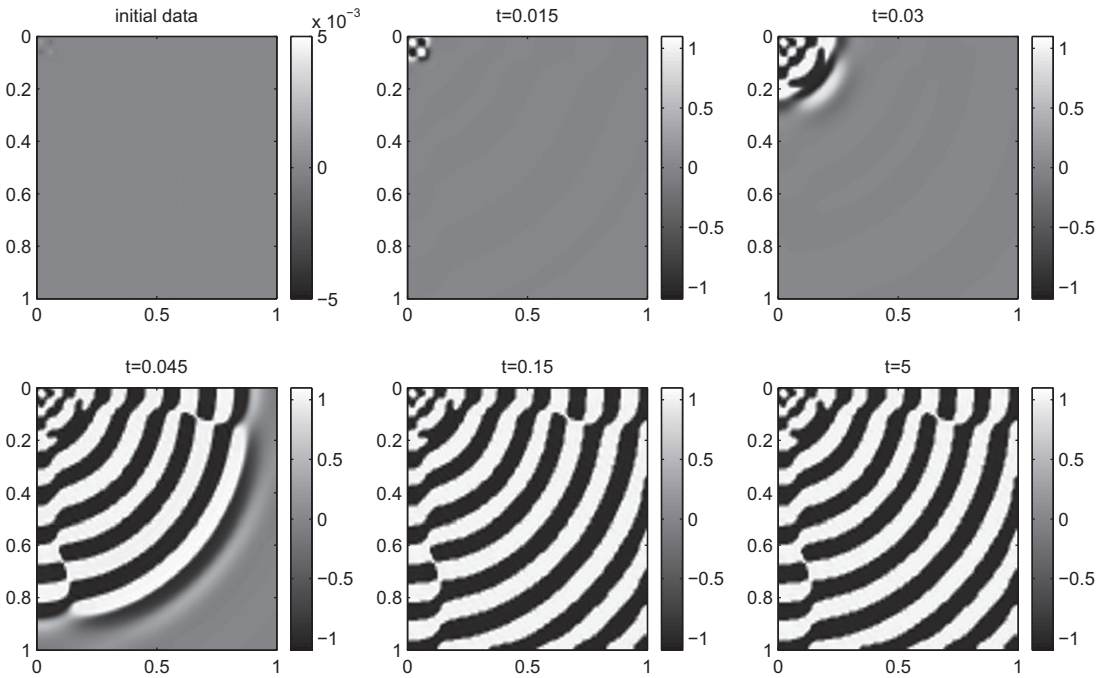

Fig. 5. The phase evolution of Example III. For the initial value, the perturbation is near the origin.

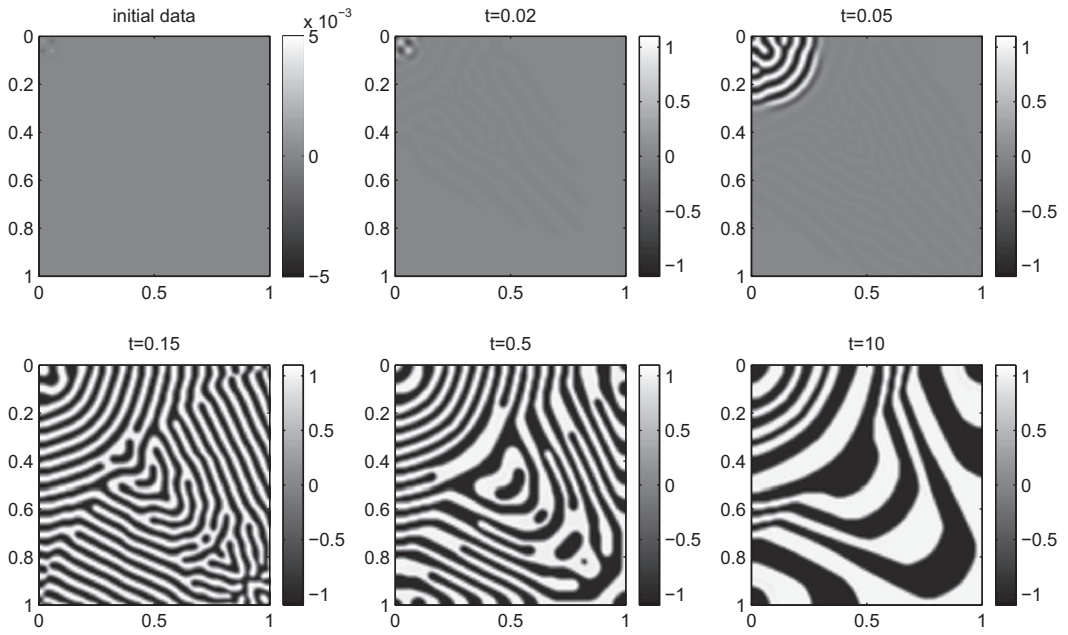

Fig. 6. The phase evolution of Example IV. For the initial value, the perturbation is near the origin.

Example III. In this example, $\varepsilon^2 = 10^{-6}$, $\gamma = 1$, and $\kappa = 1$. For the initial value,

$$\varsigma = 10^{-3} G(x, y, 0, 0, 8h).$$

In this example, the density of the interfacial energy is much smaller than previous two examples. According to Fig. 5, the spinodal decomposition took place, but the phase transition stopped before the coarsening process.

Example IV. In this example, $\varepsilon^2 = 10^{-6}$, $\gamma = 0.1$, and $\kappa = 1$. For the initial value,

$$\varsigma = 10^{-3} G(x, y, 0, 0, 8h).$$

The data are almost the same as those for Example III, except the bulk energy for Example IV is one tenth of that of Example III. In some sense, the density of interfacial energy for Example IV is amplified. In this example, we can observe the typical phase transition phenomena (see Fig. 6).

5. Concluding remarks

In this paper, we gave a fully discretized scheme for an initial boundary value problem frequently encountered with the Cahn–Hilliard equation. We made use of a semi-implicit scheme in the temporal variable, and we established that the energy property can be expected to be preserved without the inconvenience of nonlinearity in discretization. We made use of a nonconforming finite element method for the fourth-order problem, which allowed us to discretize the fourth-order problem directly with finite element spaces of lower-order continuity. The method can be used for other similar fourth-order evolution problems.

We presented some numerical examples to illustrate the effectiveness of the method. The typical phenomena were observed on fixed triangulation, even when ε is small. (Indeed, the cases in which ε is small are important in application, and the small ε would bring in subtleties in computation. We refer to [32] for some analysis.) The evolution of the phase and the energies demonstrated the mechanism of the phase evolution and the competition between the bulk energy and the interfacial energy. Particularly, in phase separation stage, the bulk energy was dominant, while in the coarsening stage, the interfacial energy was dominant.

The method is well suited for solving the steady-state equation of the system, namely the limit equation of Cahn–Hilliard equation. Indeed, the steady-state equation is nonlinear, and a fundamental method to solve such an equation is to treat the solution as a limit of a solution of corresponding evolutionary equation. As the solution of the Cahn–Hilliard equation will tend to a limit, addressing the long-time behavior of the numerical method is of central importance to the computation of the steady-state equation.

So far, the mesh and all parameters in the computation are fixed. It would be possible to make use of adaptive methods in both spatial and temporal triangulation, and in the parameters. The examples in Section 4 indicated that the time scales for the two stages are different; therefore, if we are interested in the long-time result, the time step could be loosened in long time. However, since the continuity of the solution in time at the beginning is subtle, we have to consider carefully the effect of a smaller time scale near the origin.

The scheme can be used to examine the phase transition in other physical backgrounds. Furthermore, we have observed several typical phenomena, and this can form a basis for more insights from physical models and mathematical theory with a view to finding typical initial and boundary conditions. The accuracy of the scheme used upon the Cahn–Hilliard equation will be discussed in the forthcoming works. Numerical experiments would be designed to test the scheme incidentally. The theoretical analysis of the scheme, which is absent so far, will depend on a deeper understanding of the Lax equivalence theorem and of the structure of the solution of the model problem. It will also be interesting to study the nonconforming element based method with the second-order scheme in time, such as the schemes reported in [29,37].

Acknowledgement

This study was supported by the National Natural Science Foundation of China (10871011).

References

[1] T. Antal, M. Droz, J. Magnin, A. Pekalski, Z. Racz, Formation of Liesegang patterns: simulations using a kinetic Ising model, Journal of Chemical Physics 114 (2001) 3770–3775.
[2] J.W. Barrett, J.F. Blowey, Finite element approximation of an Allen–Cahn/Cahn–Hilliard system, IMA Journal of Numerical Analysis 22 (2002) 11–71.
[3] A. Bertozzi, S. Esedoglu, A. Gillette, Inpainting of binary images using the Cahn–Hilliard equation, IEEE Transactions on Image Processing 16 (2007) 285–291.
[4] J. Cahn, On spinodal decomposition, Acta Metallurgica 9 (1961) 795–801.
[5] J. Cahn, J. Hilliard, Free energy of a nonuniform system. I. Interfacial free energy, Journal of Chemical Physics 28 (1958) 258–267.
[6] L. Chen, J. Shen, Applications of semi-implicit Fourier-spectral method to phase field equations, Computer Physics Communications 108 (1998) 147–158.
[7] S.M. Choo, S.K. Chung, Conservative nonlinear difference schemes for the Cahn–Hilliard equation, Computers and Mathematics with Applications 36 (1998) 31–39.
[8] S.M. Choo, S.K. Chung, K.I. Kim, Conservative nonlinear difference scheme for the Cahn–Hilliard equation, Computers and Mathematics with Applications 39 (2000) 229–243.
[9] S.M. Choo, Y.J. Lee, A discontinuous Galerkin method for the Cahn–Hilliard equation, Journal of Applied Mathematics and Computing 18 (2005) 113–126.
[10] M.I.M. Copetti, C.M. Elliott, Numerical analysis of the Cahn–Hilliard equation with a logarithmic free energy, Numerische Mathematiek 63 (1992) 39–65.
[11] Q. Du, R.A. Nicolaides, Numerical analysis of a continuum model of phase transition, SIAM Journal on Numerical Analysis 28 (1991) 1310–1322.
[12] G. Dziuk, C.M. Elliott, Surface finite elements for parabolic equations, Journal of Computational Mathematics 25 (2007) 385–407.
[13] C. Elliott, The Cahn–Hilliard model for the kinetics of phase separation, in: J. Rodrigues (Ed.), Mathematical Models for Phase Change Problems, International Series of Numerical Mathematics, vol. 88, Birkhäuser, Basel, 1989.
[14] C. Elliott, D. French, Numerical studies of the Cahn–Hilliard equation for phase separation, IMA Journal of Applied Mathematics 38 (1987) 97–128.
[15] C.M. Elliott, D.A. French, A non-conforming finite element method for the two-dimensional Cahn–Hilliard equation, SIAM Journal on Numerical Analysis 26 (1989) 884–903.
[16] C.M. Elliott, D.A. French, F.A. Milner, A second-order splitting method for the Cahn–Hilliard equation, Numerische Mathematiek 54 (1989) 575–590.
[17] C.M. Elliott, S. Larsson, Error estimates with smooth and nonsmooth data for a finite element method for the Cahn–Hilliard equation, Mathematics of Computation 58 (1992) 603–630.
[18] C.M. Elliott, S. Zheng, On the Cahn–Hilliard equation, Archive for Rational Mechanics and Analysis 96 (1986) 339–357.
[19] D.J. Eyre, An unconditionally stable one-step scheme for gradient systems, preprint, 1997.
[20] X. Feng, O.A. Karakashian, Fully discrete dynamic mesh discontinuous Galerkin methods for the Cahn–Hilliard equation of phase transition, Mathematics of Computation 76 (2007) 1093–1117.
[21] X. Feng, A. Prohl, Error analysis of a mixed finite element method for the Cahn–Hilliard equation, Numerische Mathematik 99 (2004) 47–84.
[22] X. Feng, A. Prohl, Numerical analysis of the Cahn–Hilliard equation and approximation for the Hele–Shaw problem, Interfaces and Free Boundaries 7 (2005) 1–28.
[23] X. Feng, H. Wu, A posteriori error estimates and an adaptive finite element algorithm for the Cahn–Hilliard equation and the Hele–Shaw flow, Journal of Computational Mathematics 26 (2008) 767–796.
[24] D.A. French, S. Jensen, Long-time behaviour of arbitrary order continuous time Galerkin schemes for some one-dimensional phase transition problems, IMA Journal of Numerical Analysis 14 (1994) 421–442.
[25] D.A. French, J.W. Schaeffer, Continuous finite element methods which preserve energy properties for nonlinear problems, Applied Mathematics and Computation 39 (1990) 271–295.
[26] D. Furihata, Finite difference schemes for $\frac{\partial u}{\partial t} = (\frac{\partial}{\partial x})^{\alpha} \frac{\delta G}{\delta u}$ that inherit energy conservation or dissipation property, Journal of Computational Physics 156 (1999) 181–205.
[27] D. Furihata, A stable and conservative finite difference scheme for the Cahn–Hilliard equation, Numerische Mathematik 87 (2001) 675–699.
[28] H. Garcke, T. Preusser, M. Rumpf, A. Telea, U. Weikard, A phase field model for continuous clustering on vector fields, IEEE Transactions on Visualization and Computer Graphics 7 (2001) 230–241.
[29] Y. He, Y. Liu, T. Tang, On large time-stepping methods for the Cahn–Hilliard equation, Applied Numerical Mathematics 57 (2007) 616–628.
[30] J. Kim, K. Kang, J. Lowengrub, Conservative multigrid methods for Cahn–Hilliard fluids, Journal of Computational Physics 193 (2004) 511–543.
[31] J.S. Langer, M. Bar-on, H.D. Miller, New computational method in the theory of spinodal decomposition, Physical Review A 11 (1975) 1417–1429.
[32] T. Nilssen, X. Tai, R. Winther, A robust nonconforming H^2-element, Mathematics of Computation 70 (2001) 489–505.
[33] B.P. Vollmayr-Lee, A.D. Rutenberg, Fast and accurate coarsening simulation with an unconditionally stable time step, Physical Review E 68 (2003) 066703.
[34] E.V.L. de Mello, O.T. da Silveira Filho, Numerical study of the Cahn–Hilliard equation in one, two and three dimensions, Physica A 347 (2005) 429–443.
[35] K.B. Rundman, J.E. Hilliard, Early stages of spinodal decomposition in an aluminum–zinc alloy, Acta Metallurgica 15 (1967) 1025–1033.
[36] P. Sheng, T. Qian, X. Wang, Continuum modelling of nanoscale hydrodynamics, in: Z. Tang, P. Sheng (Eds.), Nanoscale Phenomena, Lecture Notes in Nanoscale Science and Technology, Springer, New York, 2007.

[37] Z.Z. Sun, A second-order accurate linearized difference scheme for the two-dimensional Cahn–Hilliard equation, Mathematics of Computations 64 (1995) 1463–1471.
[38] M. Wang, Z. Shi, J. Xu, A new class of Zienkiewicz-type nonconforming element in any dimensions, Numerische Mathematik 106 (2007) 335–347.
[39] G.N. Wells, E. Kuhl, K. Garikipati, A discontinuous Galerkin method for the Cahn–Hilliard equation, Journal of Computational Physics 218 (2006) 860–877.
[40] Y. Xia, Y. Xu, C.W. Shu, Local discontinuous Galerkin methods for the Cahn–Hilliard type equations, Journal of Computational Physics 227 (2007) 472–491.
[41] Y. Xia, Y. Xu, C.W. Shu, Application of the local discontinuous Galerkin method for the Allen–Cahn/Cahn–Hilliard system, Communication in Computational Physics 5 (2009) 821–835.
[42] C. Xu, T. Tang, Stability analysis of large time-stepping methods for epitaxial growth models, SIAM Journal on Numerical Analysis 44 (2006) 1759–1779.
[43] X. Ye, The Fourier collocation method for the Cahn–Hilliard equation, Computers and Mathematics with Applications 44 (2002) 213–229.
[44] X. Ye, The Legendre collocation method for the Cahn–Hilliard equation, Journal of Computational and Applied Mathematics 150 (2003) 87–108.
[45] X. Ye, X. Cheng, The Fourier spectral method for the Cahn–Hilliard equation, Applied Mathematics and Computation 171 (2005) 345–357.
[46] S. Zhang, M. Wang, A posteriori estimator of nonconforming finite element method for fourth order elliptic perturbation problems, Journal of Computational Mathematics 26 (2008) 554–577.
[47] J. Zhu, L. Chen, J. Shen, V. Tikare, Coarsening kinetics from a variable-mobility Cahn–Hilliard equation: application of a semi-implicit Fourier spectral method, Physical Review E 60 (1999) 3564–3572.